

An Embedded Feature Selection Framework for Control

Jiawen Wei*
Central South University
Changsha, Hunan, China
jiawennw@gmail.com

Fangyuan Wang*
Zhejiang Sci-Tech University
Hangzhou, Zhejiang, China
wfy11235813@gmail.com

Wanxin Zeng
Central South University
Changsha, Hunan, China
194611090@csu.edu.cn

Wenwei Lin
Central South University
Changsha, Hunan, China
linwweix@gmail.com

Ning Gui†
Central South University
Changsha, Hunan, China
ninggui@gmail.com

ABSTRACT

Reducing sensor requirements while keeping optimal control performance is crucial to many industrial control applications to achieve robust, low-cost, and computation-efficient controllers. However, existing feature selection solutions for the typical machine learning domain can hardly be applied in the domain of control with changing dynamics. In this paper, a novel framework, namely the Dual-world embedded Attentive Feature Selection (D-AFS), can efficiently select the most relevant sensors for the system under dynamic control. Rather than the one world used in most Deep Reinforcement Learning (DRL) algorithms, D-AFS has both the real world and its virtual peer with twisted features. By analyzing the DRL's response in two worlds, D-AFS can quantitatively identify respective features' importance towards control. A well-known active flow control problem, cylinder drag reduction, is used for evaluation. Results show that D-AFS successfully finds an optimized five-probes layout with 18.7% drag reduction than the state-of-the-art solution with 151 probes and 49.2% reduction than five-probes layout by human experts. We also apply this solution to four OpenAI classical control cases. In all cases, D-AFS achieves the same or better sensor configurations than originally provided solutions. Results highlight, we argued, a new way to achieve efficient and optimal sensor designs for experimental or industrial systems. Our source codes are made publicly available at <https://github.com/G-AILab/DAFSfluid>.

CCS CONCEPTS

• **Computing methodologies** → **Feature selection; Reinforcement learning; Knowledge representation and reasoning.**

*Both authors contributed equally to this research.

†Corresponding Author.

Permission to make digital or hard copies of all or part of this work for personal or classroom use is granted without fee provided that copies are not made or distributed for profit or commercial advantage and that copies bear this notice and the full citation on the first page. Copyrights for components of this work owned by others than ACM must be honored. Abstracting with credit is permitted. To copy otherwise, or republish, to post on servers or to redistribute to lists, requires prior specific permission and/or a fee. Request permissions from [permissions@acm.org](https://permissions.acm.org).

Conference'22, August 2022, Washington, DC, USA

© 2022 Association for Computing Machinery.

ACM ISBN 978-x-xxxx-xxxx-x/YY/MM... \$15.00

<https://doi.org/10.1145/nnnnnnn.nnnnnnn>

KEYWORDS

Deep Reinforcement Learning, Feature Selection, Optimal Sensor Placement

ACM Reference Format:

Jiawen Wei, Fangyuan Wang, Wanxin Zeng, Wenwei Lin, and Ning Gui. 2022. An Embedded Feature Selection Framework for Control. In *Proceedings of ACM Conference (Conference'22)*. ACM, New York, NY, USA, 10 pages. <https://doi.org/10.1145/nnnnnnn.nnnnnnn>

1 INTRODUCTION

For experimental and industrial systems, reducing sensor requirements while maintaining optimal control performance is crucial for human experts to understand target systems and potentially transpose these techniques to industrial cases. It is one of human beings' most critical intellectual activities, i.e., extracting knowledge from unknown environments to recognize and exploit the world[33]. To better understand the target system, scientists/engineers use intuition and domain knowledge to identify critical information based on continuous observations of system performance[18]. But for a complex system with massive sensory inputs, this handcrafted solution through trial-and-error is normally time-consuming, costly, and heavily reliant on human expertise. Thus, it is vital to develop an effective and systematic solution to identify relevant sensors without or with minimal human intervention.

Nowadays, DRL has shown great success in complex system control problems[21] by combining reinforcement learning and deep learning[22]. The introduction of Deep Neural Networks (DNN) can extract important features from a huge set of raw inputs. Despite its success, the opaque nature of DNN hides the critical information about which sensors are most relevant for control[12, 29]. Existing solutions for sensor selection under DRL have been limited to the recursive sensor set selection and evaluation with certain heuristic algorithms[24]. As their complexity increases rapidly with the number of candidate sensors, these methods are inapplicable for systems with massive possible inputs.

This requirement is similar to the Feature Selection (FS) problem in Machine Learning(ML) [20], also known as variable selection or attribute selection. This process aims to select a subset of relevant features with respect to the modeling labels. However, due to the distinctiveness of control process, choosing a suitable variable as a label is very troublesome. For example, Fig. 1 shows a classic flow control problem to reduce the drag and lift of a cylinder by adjusting flow injection/suction with two jets(represented by two red dots)

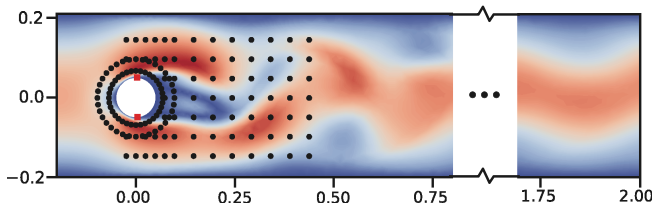


Figure 1: Instantaneous velocity flow field with 151 probes. Black dots represent sensor locations and colors represent velocity(fields).

and 151 probes. Firstly, the immediate reward corresponding to the time series state set is often meaningless as a label. The instance injection/suction might not change the immediate reward significantly. Secondly, the goal for control typically uses the discounted cumulative return as a loss function that often has long and uncertain latency and has little relevance to the single-step state. Thus, neither immediate reward nor cumulative return is appropriate as the mandatory training label in most feature selection methods. In later experiments, we also experimentally prove that existing feature selection methods are not suitable in systems with control.

For effective control, a DRL controller has already learned the relevance of different inputs during its exploration and exploitation. Can we make the hidden knowledge on the relevance of respective sensors explicit and provide qualitative evaluation during DRL training? To address this challenge, we propose a new solution, the Dual-world based Attentive embedded Feature Selection(D-AFS), a general mechanism that enables the DRL controller to interact with the real world and its virtual peer with twisted features. Our method combines general DRL framework and feature selection module, which can identify the contribution of inputs simultaneously with strategy learning process. In summary, our contributions are:

- **A new direction for embedded feature selection in control:** We combine the exploration and exploitation capabilities of DRL with an attention-based feature evaluation module, that qualitatively evaluates the impact of different features by translating feature weight calculation to feature selection probability problem. The method can identify the feature importance of unknown systems for control during DRL’s strategy learning process.
- **A dual-world architecture design:** We propose a dual-world architecture that includes real world and virtual world, of which the virtual world is mapped from its real peer by the feature evaluation module. Dual-world enables D-AFS complete feature importance ranking without jeopardizing DRL’s strategy exploration.
- **Excellent results on active flow control:** We apply D-AFS with the Proximal Policy Optimization (PPO) algorithm[31] in the case mentioned above. D-AFS/PPO successfully reduces a five-sensor layout from 151 possible probes, with a drag coefficient of 2.938, very close to the theoretical limit of 2.93 without vortex shedding, and achieves 18.7% drag reduction than the state-of-the-art solutions using 151 probes.

We also successfully adapt Deep Q-Network(DQN)[22] and Deep Deterministic Policy Gradient (DDPG)[21] into D-AFS, apply them

on four OpenAI Gym[6] classical control cases. In all cases, D-AFS selects the same or better sensor subsets than the original expert-based solutions (Gym provided). Results clearly show that our solution can effectively identify system key sensors, improve the interpretability of the target system and reduce the reliance on human expertise.

2 RELATED WORK

This section discusses the related work from two aspects: 1) The feature selection methods in machine learning; 2) The abbreviated research for sensor selection in active flow control.

2.1 Feature Selection in ML

Feature selection is a technology that contains automatically discovering, evaluating, and selecting relevant features[3]. Generally, it can be divided into three categories[20]: 1) Filter methods separate feature selection from the learning process and only rely on the measures of the general characteristics of the training data to evaluate the feature weights. Different feature selection algorithms exploit various types of criteria to define the relevance of features, e.g., Fisher score[13] and ReliefF[28]. 2) Wrapper methods[35] predict accuracy of a predefined learning algorithm to evaluate the quality of recursive selected features. They normally suffer high computation costs and low scalability. 3) Embedded methods depend on the interactions with the learning algorithm and evaluate feature sets according to the interactions. The most recent approaches are in this class e.g., XGBoost[9], LightGBM[17] and Random Forest(RF)[4]. Recently, DNN-based solutions are proposed, e.g., the attention-based, AFS[14] or casualty-based [37]. However, trajectories generated by the DRL controller do not follow the independent and identically distributed assumption, making it impossible to directly transfer and use the feature selection methods in the ML domain. [16] creates virtual sensors to do fault detection by using existing sensors and applying domain knowledge to the data. However, this approach does not actually reduce the number of sensors and cannot be applied to control tasks. As pointed out in the introduction, for model-free systems, it is challenging to provide appropriate labels for each system state, as demanded in most ML feature selection approaches. Thus, it is difficult for existing ML feature selection methods to be applied in the DRL control environment.

2.2 Optimal Sensor Placement in Flow Control

The issue of optimal sensor placement has been investigated with certain domain-specific knowledge. Most existing solutions, e.g., [5, 11] are based on compressed sensing theory that selects a limited number of sensors that can effectively perform flow reconstruction. These approaches do not depend on the learning algorithm and can be seen as a special filter feature selection algorithm. This stream of methods also has very high computation complexity, as we need to reconstruct the whole flow. Furthermore, as stressed by Stephan & Simon [23], control does not systematically require faithful flow reconstruction. The partial knowledge of relevant ‘hidden’ variables may be sufficient.

Despite its success in many domains, only in the recent work of Rabault et al. [26], DRL has been used to control the flow past a 2D cylinder. They use 151 probes to learn control strategy by PPO in

the 2D Kármán Vortex Street simulation. Tang et al. [34] further improve their work through extending the Reynolds numbers range and sensor observations. These researches have not yet involved the optimization of sensor selection. Paris et al. [24] recently proposes a sensor selection algorithm based on a well-trained PPO controller. However, this approach adopts the so-called wrapper method by evaluating different combinations of features. Their work has very high computation complexity, and their discussion is limited to a system with 15 probes.

To the best of our knowledge, there have been no systematic solutions yet to obtain interpretable environmental representations through the learning and exploration processes of DRL.

3 DEFINITIONS AND NOTATIONS

This section gives a general definition of the problem studied in this paper and briefly demonstrates the related notations.

Raw Features. Given a controlled object, the basic observations are a set of states periodically collected by sensors deployed in the system. We use $\mathcal{S}_r = \{s^k | k = 1, 2, \dots, m\}$ to describe the set of raw states, where k represents the number of sensors.

Feature Selection for Control. The goal of feature selection for control under the DRL framework is stated as follows. Given a set of features \mathcal{S}_r from the real world, find a subset of features, $\mathcal{S}^* \subseteq \mathcal{S}_r$, to maximize the expected cumulative return \mathcal{R}_t for a given DRL algorithm. As shown in Eq. (1):

$$\mathcal{S}^* = \arg \max_{\mathcal{S}_r} \mathcal{R}_t = \arg \max_{\mathcal{S}_r} \sum_t^{\infty} \gamma^t r_t \quad (1)$$

where γ is a discount rate.

Discussion. For a target system, if a well-designed controller is capable of achieving effective control, the raw features must contain all the necessary information for control. However, it has been wildly agreed that reducing sensor requirements while keeping optimal control performance is crucial to many industrial control applications to achieve robust, low cost, and computation efficient controllers[18]. Previous works on the industrial control with DRL[24] demonstrate that when the selected feature representation matches the form required by the physical model, the DRL controller can usually even achieve a better control effect. This characteristic is of vital importance in understanding the underlying physical model of the target systems.

4 PROPOSED METHOD

In this section, the overall structure of D-AFS and the mechanism of embedded feature selection are illustrated and analyzed.

4.1 Design Principles

The basic design principle for two different worlds is rather straightforward. Firstly, if a feature is irrelevant or weakly related to the system, it has little effect on a “good” control strategy. Conversely, a feature strongly related to the physical model of the system or the control goal should have a pronounced impact on the control strategy. Generally, the one that is more benign for the controller might have more impacts.

However, the dual-world design brought a series of problems to the existing DRL solutions with only one world. Three main

issues need to be tackled: 1) How to effectively combine the real and virtual world without affecting the normal operation of DRL? 2) How to dynamically adjust the combination of features in the virtual world space without jeopardizing the DRL learning process? 3) How to modify existing DRL algorithms to allows online feature evaluation?

Thus, we introduce the dual-world architecture, which contains three main modules, the environment module, the evaluation module, and the DRL module, as shown in Fig. 2. The environment and the DRL module are inherited directly from the original DRL framework, but detailed designs are slightly different to support the two worlds. The evaluation module calculates the importance of each feature through the attention mechanism and then helps generate the virtual world. The DRL module, evaluation module, and the unique dual-world system are loosely coupled in the architecture we designed. We minimize the modification of the general structure of traditional DRL algorithms and maintain its integrity to the greatest extent, which significantly promotes the reuse of the existing state-of-the-art DRL algorithms. Therefore, the DRL module can be determined according to the specific problem.

4.2 Dual-world

We first need to clarify the different roles between the real world and the virtual world of the dual-world space. On the one hand, we need the real world to provide system information to explore the correct control strategy. On the other hand, the virtual world searches for the optimal features and representations by continuously tuning the mapping from the real world to the virtual world. The real world features are the system’s original features \mathcal{S}_r , which is used to interact with the policy of the DRL module. And the virtual world is the real world mapping through the evaluation module, which can be used to evaluate the validity of the selected features. The mapping function is generated with the attention-based evaluation module illustrated in the following section. In D-AFS, the environment is the combination of the real and virtual world $\mathcal{S}_r \cup \mathcal{S}_v$.

4.3 Attention-based Evaluation Module

The attention-based evaluation (AE for short) module aims to evaluate the importance of different features by assigning different weights (denoted as P). The structure of AE is shown in the green area in Fig. 2.

The AE module is a revised attention mechanism extended from our previous work[14]. This module consists of two key components, a dense network E with N_E neuronal units and several Attention Networks (AN for short) for calculating the importance weights of each input.

The dense network $E = \tanh(\mathcal{S}_r^T \mathbf{W}_E + \mathbf{b}_E)$, $\mathbf{W}_E \in \mathbb{R}^{m \times N_E}$, $\mathbf{b}_E \in \mathbb{R}^{N_E}$, is used to abstract the internal relationship between the inputs \mathcal{S}_r . \mathbf{W}_E and \mathbf{b}_E are parameters, nonlinear function $\tanh(\cdot)$ keeps positive and negative values. To some extent, the dense network can reduce the redundancy of all sensors, of which the units N_E can be adjusted according to respective inputs.

Once we have extracted the relationship of features by E , we configure an attention network for each feature to generate weight separately. We do not adopt the typical soft attention mechanism

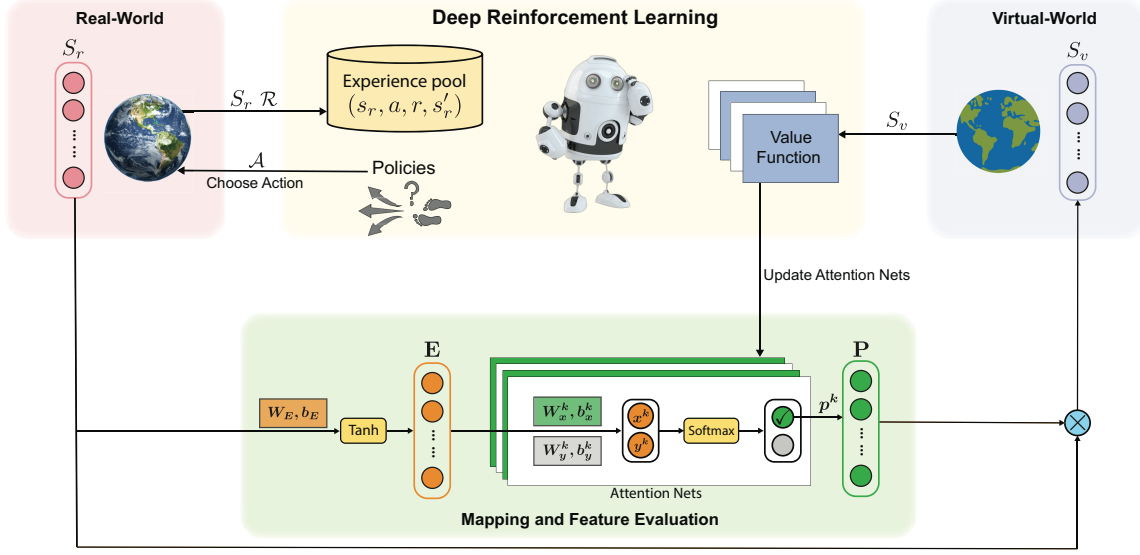


Figure 2: The overall architecture of D-AFS with the “real” and “virtual” world environment, the evaluation module and the DRL module. The virtual world is mapped from the real world. DRL learns in two mixed worlds, explores the correct control strategy in the real world, and provides evaluation information for feature selection in the virtual world.

to generate a weighted arithmetic mean of all features. This operation might result in small weights for most features and large weights for a tiny number of features and suffer the loss of details on the whole feature sets. These weights can determine whether one feature should be selected or not. More detailed, it generates two values, $X = EW_x + b_x$ and $Y = EW_y + b_y$, to represent the selected/unselected probability of a feature, respectively. In general, the higher the weight of the feature being selected (X), the more important the feature is for control. Then we use the softmax function to magnify the distance between selected and unselected.

$$p^k = \frac{\exp(x^k)}{\exp(x^k) + \exp(y^k)}, x^k \in X, y^k \in Y \quad (2)$$

Finally, these attention nets will generate a matrix of attention weights $P = \{p^k | k = 1, 2, \dots, m\}$, which has the same dimension as features. With Eq. 3, we generate a feature representation of the virtual world with S_v multiplied by attention weights.

$$S_v = S_r \odot P \quad (3)$$

The AE module generates a dynamic mapping function that maps representations from the real world S_r to the virtual world S_v , which will be used for DRL to update the strategy. Additionally, with the attention weights matrix P generated by AE, we can evaluate respective features when DRL has explored an efficient strategy.

4.4 PPO in Dual-world

As far as we know, value functions are used in one way or another among the current model-free DRL algorithms[1]. In our algorithm, in addition to the role of the original DRL algorithm, the value function also needs to guide the AE module to select valuable features during the training process. This subsection shows how to integrate the D-AFS with the popular Proximal Policy Optimization(PPO)

algorithm, denoted as D-AFS/PPO. PPO is a popular policy-based online algorithm with clipped probability ratios that forms a lower bound of the performance of the policy. In order to allow the agent to interact with the environment correctly, we use the real world as the input of the PPO actor network, which is the same as the original PPO algorithm. Thus, the actor network with parameters θ can be updated by:

$$\theta^* = \arg \max_{\theta} L^{CLIP}(\theta) \quad (4)$$

where,

$$L^{CLIP}(\theta) = \mathbb{E}_t[\min(r_t(\theta), \text{clip}(r_t(\theta), 1 - \epsilon, 1 + \epsilon))A^{\pi_{\theta t}}(s_r, a)],$$

$r_t(\theta)$ is the probability ratio of the old and the new policy, the subscript t is the number of iteration.

The difference is that in our algorithm, we use the virtual world as the input of the critic network, allowing the critic network to evaluate the goodness of the selected features of the evaluation module while scoring the performance of the actor network. That is:

$$\phi^*, \psi^* = \arg \min_{\phi, \psi} \mathbb{E}_t(V_{\phi, \psi}(s_v) - \mathcal{R}_t)^2 \quad (5)$$

ϕ and ψ are parameters of critic network and attention module, respectively. $V_{\phi, \psi}(s_v)$ is value function and \mathcal{R}_t is accumulative return.

The detailed structure of this D-AFS/PPO is shown in Algorithm 1. The bold pseudo-codes are the revised parts to support the dual-world DRL learning.

5 EXPERIMENTS AND ANALYSIS

In this section, the experimental system and settings are firstly introduced. Then the results for both FS solutions and DRL solutions are provided and analyzed. We also briefly provide further experiments in OpenAI Gym to demonstrate D-AFS’s adaptability.

Algorithm 1 D-AFS/PPO, Actor-Critic based

Initial parameters of actor network θ_0 , critic network ϕ_0 and attention network ψ_0 .

for $t = 1, 2, \dots$ **do**

Run policy $\pi(\theta_t)$ to get trajectories $\mathcal{D}_t(s_r, a, r, s_r')$

Compute accumulative return \mathcal{R}_t

Compute attention weights p based on Eq. (2)

Compute $s_v \leftarrow s_r \odot p$

Compute advantage estimates A_t based on current function $V_{\phi_t, \psi_t}(s_v)$

Update the actor network by maximizing the PPO-Clip based on Eq. (4) with Adam $\theta_{old} \leftarrow \theta$

Update the critic network by regression on MSE based on Eq. (5) with Adam $\{\phi_{old} \leftarrow \phi, \psi_{old} \leftarrow \psi\}$

end for

5.1 System Description and Settings

Drag reduction and active flow control are critical technologies in the fluid industry. Here, we briefly introduce the target system and experiment settings.

Target System: This environment is from a well-known benchmark [30] which consists of a cylinder of diameter $D = 0.1$ immersed in a constant flow of a box of total length $L = 2.2$ and height $H = 0.41$. The cylinder is slightly downward from the center of the Y-Axis by 0.005. The mean velocity magnitude is $\bar{U} = 1$. And the Reynolds number based on the mean velocity magnitude and cylinder diameter ($Re = \bar{U}D/\nu$, with ν the kinematic viscosity) is set to $Re = 100$. When the target system is in an unstable state, the flow velocity and pressure of the wake behind the cylinder show periodic changes due to the transmission of the vortex street. As the learning of the control strategy becomes effective, the velocity and the pressure of the wake gradually decrease.

Two synthetic jets are located at the top/bottom extremities of the cylinder, which we can use DRL to control, as indicated in Fig. 3 with solid red dots. There are 151 velocity probes placed around the cylinder and the near wake, which provide the network with a relatively detailed flow description, as indicated in Fig. 3 with black dots. Circle and Square are Top5 and Top11 probes selected by human experts. Our experimental environment is inherited from [26]. Detailed settings and calculations can refer to the paper.¹

D-AFS/PPO Settings: Due to the limited continuous action space of the 2D flow control system, we use Beta policy[10], which has finite support and no probability density that falls outside the boundary, to sample actions in the training process and use deterministic policy in the testing process. It is also the default policy of Tensorforce[19] for limited continuous action space, which is used by [27]. The critic network consists of 4 layers: an input layer, two hidden layers with 512 cells, and an output layer. In the AE module, the dense network N_E has 20 cells.

The original paper[26] takes 24 hours to train a stable controller on a single CPU. And about 99.7% of the computation time is spent on the environment itself using FEniCS[2] rather than the DRL algorithm [27]. Thus, we designed the asynchronous training architecture to accelerate Algorithm 1 by syncing parameters and

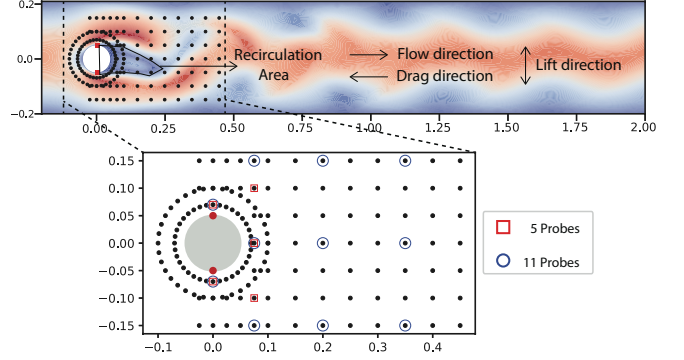


Figure 3: The 2D active flow control simulation environment without control. The location of the jets is indicated by the red dots.

averaging gradients on each worker. The architecture reduced the training time from 40 hours to 3.6 hours by using 20 threads.

Evaluation Metrics and Reward Function: We use drag coefficient C_D , lift coefficient C_L , recirculation area size, and velocity fluctuations and pressure fluctuations to evaluate the performance of a trained controller. The drag coefficient and lift coefficient are the normalized total instantaneous drag (opposite the constant flow direction) and lift (perpendicular to the constant flow direction) on the cylinder. And the recirculation area is the region in the downstream neighborhood of the cylinder where the horizontal component of the velocity is negative. To compare fairly, we use the standard PPO with the absolute same configuration for learning as the arbiter to evaluate different probe configurations.

In short, an excellent active flow control strategy means multiple evaluations, small C_D and C_L , low C_L fluctuations, pressure drop and velocity magnitude, and a large recirculation area. In this way, efficient active control can reduce vortex shedding caused by the bluff cylinder and gain a smoother flow. Here, the reward function is defined as follows:

$$r_t = -C_D - 0.2|C_L|, \quad (6)$$

which is to minimize the drag and lift to stabilize the vortex alley and the same as other papers to facilitate comparison.

In the 2D simulation of the target system, our method is applied to learn the active flow control strategy and obtain attention weights of all 151 probes sensors simultaneously. We use the attention weight from the AE module when the D-AFS/PPO controller achieves stable rewards. Then, the probes with Top K weights are used for control with the same reward function and the original PPO controller. The C_D and C_L achieved with different methods are used for evaluations.

5.2 Comparison with Other FS Methods

In this section, we test the performance of state-of-the-art baseline feature selection algorithms in their feature identification capabilities in control. We choose eight strong feature selection baselines, including classic methods, gradient boosting methods and recent population-wise methods. We also provide one instance-wise feature selection method. Implementation of these algorithms are

¹<https://github.com/jerabaul29/Cylinder2DFlowControlDRL>

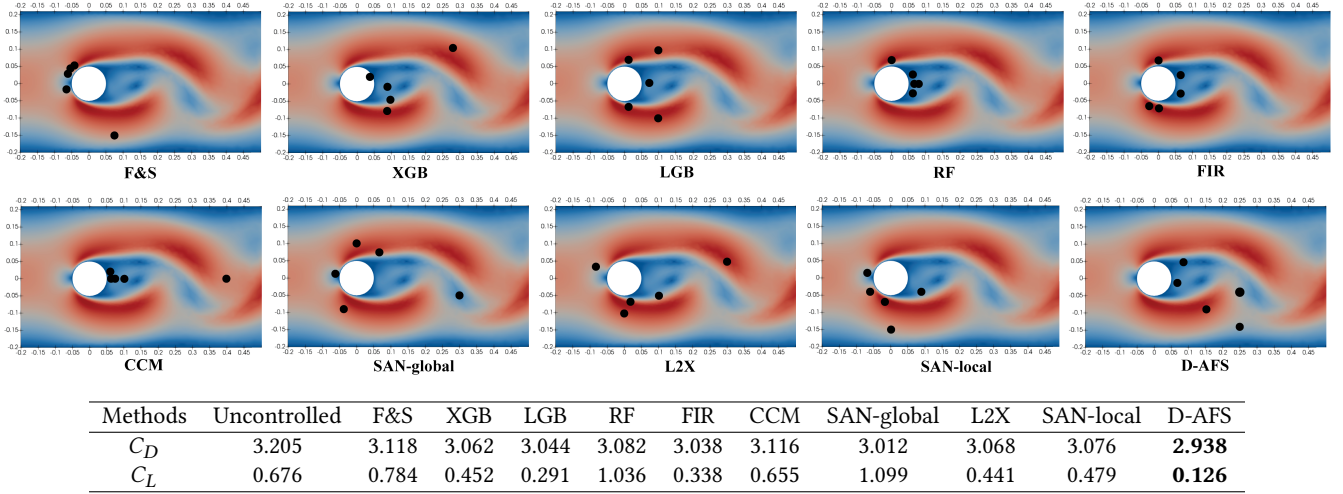


Figure 4: Comparison of the Top 5 probes selected with different feature selection solutions. Table shows the average values of the drag coefficient C_D and lift coefficient C_L when the control strategy converges with only the selected five probes with the PPO controller

either by the scikit-learn package[25] or from codes with their original papers. **F&S** [13], short for Fisher Score, a similarity-based method, which selects each feature independently according to their scores under the fisher criterion. **XGB**[9], short for XGBoost, an optimized distributed gradient boosting library that can calculate the feature importance across many trees. **LGB**[17], short for LightGBM, gradient boosting framework that uses tree based learning algorithms. **RF**[15], short for Random Forest, operates by constructing a multitude of decision trees at training time. **FIR**[36], a novel dual-net architecture consisting of operator and selector for discovery of an optimal feature subset. **CCM**[8], employs kernel-based measures of independence to find a subset of covariates that is maximally predictive of the response. **SAN**[32], explores the use of attention-based neural networks mechanism for estimating feature importance. We use both the local/global variants: SAN-local and SAN-global. **L2X**[7], an instance-wise feature selection method that extract a subset of features that are most informative for each given example.

Time series sensory data and immediate rewards during the training and exploration of the PPO controller are collected to provide training data set for supervised feature selection. The data set includes 50 epochs series, with 80 control steps in each epoch.

Fig. 4 shows the Top 5 probes selected by different feature selection methods and corresponding control effects. The layouts selected by these supervised feature selection methods are not suitable for control, whether from numerical or physical perspectives. Most of them select probes whose characteristics do not change significantly during the periodic vortex shedding. Some of them, e.g. F&S, SAN, and L2X, select the probes located on the left side of the cylinder, generally seen as an ineffective area. The value of these probes generally provides little help for the drag reduction task. In order to verify their effectiveness in control, we use PPO to control systems with only Top 5 selected probe, respectively. The drag and lift coefficient in the table (bottom part of Fig. 4) do clarify that

these probes layouts cannot achieve effective active flow control behind the cylinder. In contrast, D-AFS achieve the best control effect for both C_D and C_L with the same number of probes.

5.3 Comparison with Existing DRL solutions

We verify the control performance obtained using the probe configurations selected by different DRL solutions with 151 probes and observe their results. The performance of the active flow control strategy under different configurations is shown in the upper part of Fig. 5. The numerical results for drag coefficient C_D , lift coefficient C_L and recirculation area size are shown in the bottom part of Fig. 5. In addition to TopK probe configurations, we also show the performance of Rabault et al.’s result with selected five-probe, marked as Expert(5) and a randomly selected five-probe configuration denoted as Random(5). In Random(5), the best performance in five rounds is reported. Here, other reference use similar environment but different settings, e.g. Tang [34] use four actuators instead of two, thus the result can not be directly compared. Reference [24] requires heuristic enumeration of sensor layouts with only 15 probes and has not yet been open-sourced.

The top part of the figure shows that the drag coefficient C_D varies periodically as the vortex shedding when the system is uncontrolled. The mean value of C_D is around 3.205, and the fluctuation amplitude is around 0.034. In comparison, taking the Top5/10/15 probes selected by D-AFS as observations, the PPO controller can achieve better active flow control. The C_D of D-AFS with the five-sensor is very close to, more exactly 99.73%, the ideal 2.93(denoted by dashed gray line) where no vortex shedding exists[26]. Compared with the five-sensor configuration by human experts[26], D-AFS achieves a 260% increase in the recirculation area and 49.2% drag reduction. Even compared to the state-of-the-art solution with 151 probes, our five-sensor configuration can achieve a further 18.7% drag reduction. The drag coefficient C_D of the best random selection is better than Expert(5), but the lift coefficient C_L is worse

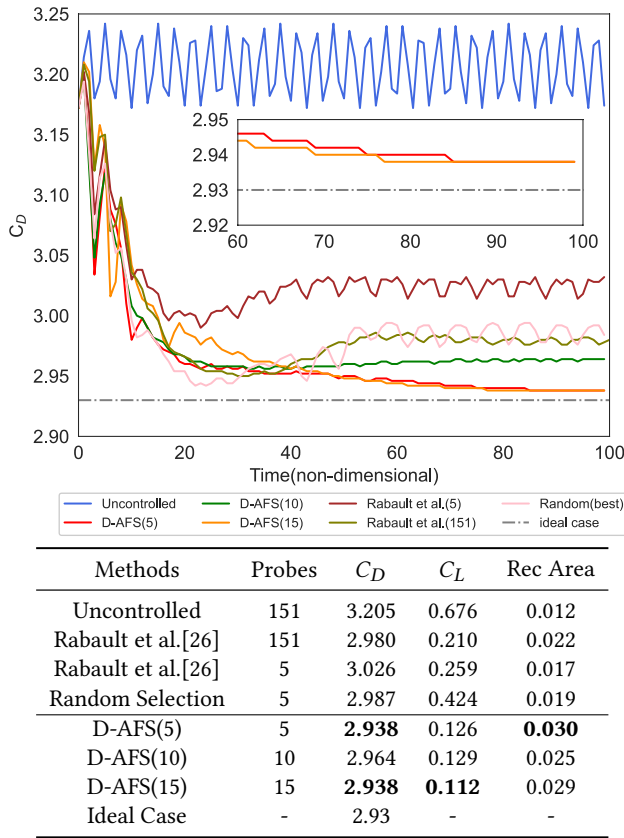


Figure 5: Time-evolutionary value of the drag coefficient C_D with different solution. Table shows the mean values of C_D , C_L and Rec Area when system becomes steady.

than the latter. That means the control strategy using randomly selected probes is unstable.

Interestingly, adding more sensors to the five-sensor layout selected by D-AFS does not bring further drag reduction, which makes this five-sensor configuration the optimized trade-off between DRL performance and sensor selection complexity. It shows that too many possibly redundant inputs may cause interference and hindrance to the controller with limited modeling capabilities, albeit they might contain more information. This finding matches precisely the finding stated in [24].

5.4 Further Analysis

In this section, we provide further analysis on the probe weight distribution, control effect analysis, impacts of different probe configurations and the complexity analysis.

Feature weight distribution: Fig. 6 illustrates the attention weight of 151 probes with different gradient colors. The darker the color, the bigger the weight and the higher the importance of the probe to the controller. We also marked the Top5, Top10, and Top15 probes with the cross, circle, and diamond. The Top5 probes selected by D-AFS are scattered behind the cylinder, and they provide an excellent ‘coverage’ of the instantaneous vortex variation, as shown in

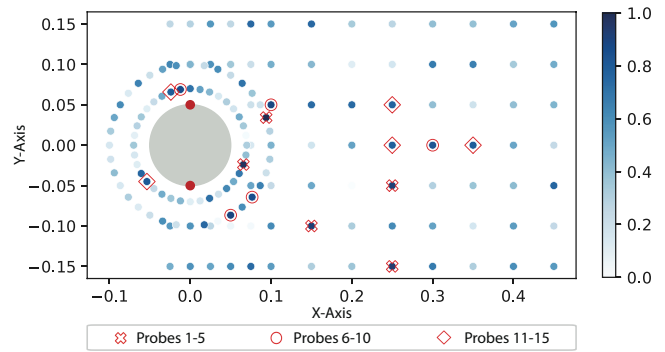


Figure 6: The attention weight distribution of 151 probes. The Top5/10/15 probes in weight ranking have been marked.

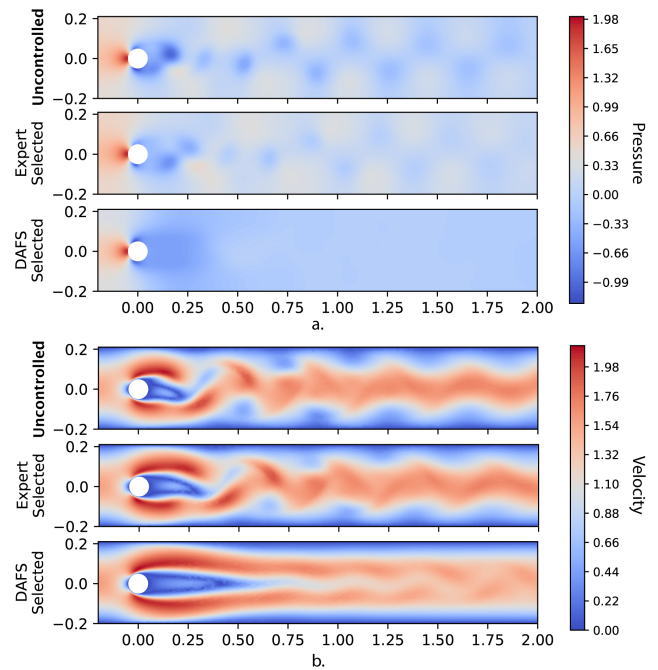


Figure 7: Comparison of active control performance(velocity and pressure) of uncontrolled and two five-probe configurations.

Fig. 8. These probes are normally critical for the control task, which can explain the selection preference of D-AFS to a certain extent. That is, probes that can deliver critical information conducive to learning will get a higher weight.

Control effect analysis: We take a look at macroscopic flow characteristics and how the active control affects them. Fig. 7 shows the snapshots of the pressure (subgraph a.) and velocity distribution(subgraph b.) under three configurations when the system enters steady states. The three configurations are Uncontrolled, Expert(5), and D-AFS(5).

The pressure distribution shows that the vortex in the wake caused by the cylinder is manifested as a significant pressure drop

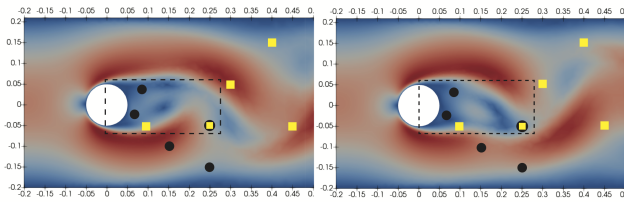


Figure 8: Identified two equivalent probe layouts with similar DRL performance, black circles and yellow squares indicate the probes selected in two separated experiments.

without active control. Similarly, the velocity magnitude fluctuates a lot, visible from the top sub-figure of the velocity distribution. The control effect from Expert(5) is shown in the middle of the two subgraphs, and we can see those probes are not in the key positions for vortex shedding. In comparison, the selected Top5 probes have good “coverage” of the instantaneous recirculation bubble. Thus, the control effect of D-AFS is much better. PPO with D-AFS(5) attenuates velocity fluctuations caused by the vortices, achieves that vortices are globally very weak and least active close to the upper and lower walls. More strikingly, the extent of the recirculation area is dramatically increased.

Equivalent probe layouts: As introduced previously, optimizing sensors’ number and location are widely demanded in various industrial domains to find cost-effective sensor solutions in redundant probes. For D-AFS, it is possible to select probes with totally different layouts because of the random exploration and exploitation nature. Fig. 8 shows two identified Top5 probes with two separated experiments, illustrated with black circles and yellow squares. They provide almost identical control performance. The drag coefficient C_D is around 2.940, the lift coefficient C_L is around 0.130.

The left and the right part of Fig. 8 are two different snapshots, which show the forward propagation of the vortex to better illustrate selected probes’ positions on the route of vortex. We can find that, although the two configurations are highly different (only one overlap), each configuration covers the key positions which contain richer information of periodic vortex shedding or located around the edge of the recirculation area. For instance, observations detected by probes located at (0.15, -0.1), (0.25, -0.15), (0.3, 0.05), (0.4, 0.15) and (0.45, -0.05) enable the DRL controller obtain rich periodic information. This also means that the control task can be converted from drag reduction to vibration reduction for these observations.

Complexity analysis: Table 1 shows the time complexity in generating feature weights for systems with different numbers of probes, ranging from 5 to 151. We also show the time when pure PPO is used for training. The settings for epochs and steps are the same as the experiment settings mentioned earlier. From this table, we can see that D-AFS generates feature weights in the process of DRL exploration and exploitation, and the overall time consumed is almost the same as that of pure PPO. The computation and resource complexity is relatively low.

In comparison, if the DRL is only used as an arbiter with a certain heuristic-guided probe configuration, e.g., [24], the computation complexity is about $O(C_n^r)$ with n are possible probes, and r are probes to select. It will increase rather fast when n and r increase.

The author pointed out that each training costs around 40 CPU hours when the system only has 12 probes. Although they provide no discussion on computation complexity, we deduce that this approach can hardly be applied to the system with 151 probes.

Table 1: The computational complexity of D-AFS and pure PPO without feature selection.(Time unit: hour)

Probes	5	10	50	100	151
PPO	3.17	3.24	3.30	3.39	3.46
D-AFS/PPO	3.19	3.28	3.37	3.49	3.60

5.5 Further Experiments in OpenAI Gym

To better explore the generalization of D-AFS, we also tune two popular DRL algorithms, DQN and DDPG into our framework. We choose four classical control cases provided by OpenAI Gym[6], including Pendulum, MountainCar, CartPole, and Acrobot, to observe control performance with feature subsets selected by D-AFS.

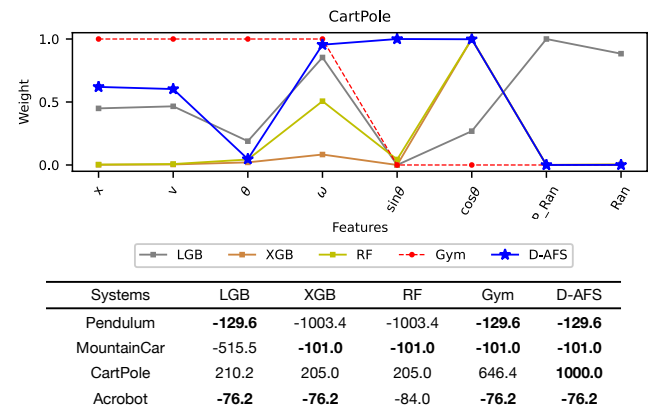


Figure 9: Comparison of controller performance with the feature subsets selected by different methods.

The lower part of Fig. 9 is a table, in which values are rewards of four systems with feature subsets selected by different methods. The larger the rewards, the better the performance of DRL’s controller. To verify that the control performance is influenced only by features, experimental settings are all the same except for the feature subsets. Results in the table show that D-AFS can select relevant features effectively and achieve the same or even better control performance than the original expert-based subsets. In Pendulum, MountainCar and Acrobot, D-AFS achieves the same rewards as Gym. Actually, it deduces the same sensor sets used with Gym in all three cases. In Cartpole, D-AFS achieves the maximum return under the limit of 1000 maximal steps in an episode, which is about 54.70% higher than the 646.4 achieved by the features provided by Gym with a different set of features. Due to the page limits, the upper part of Fig. 9 only shows the feature weights calculated by different methods for CartPole. Since the feature weight values generated by different methods are not uniform, we normalize all weights for better comparison. Regarding the features provided by Gym based

on human expertise, we set their weights to 1, while other features that are not included are set to 0. More comprehensive weights for other cases are provided in Appendix A.

6 CONCLUSION

Unlike humans who are good at learning unknown environments through interaction, the most existing DRL algorithms cannot gain explicit environmental knowledge from the learning and exploration process. In this paper, a dual-world feature selection method D-AFS is proposed to quantitatively evaluate the impacts of different inputs for control during the DRL training process. A set of experiments is performed in one classic flow control. Results show that D-AFS can effectively identify the system-mechanism-related inputs. With the deduced five-probe layout, we can achieve the best drag reduction than all other strong baselines. Results highlight, we argue, a new way to achieve efficient and optimal sensor designs for experimental or industrial systems. In this paper, our work limits to the active flow problem with limited complexity due to the high computation complexity with FEniCS for solving partial differential equations. We are working on implementing D-AFS on a deep neural network based simulator for more fast and complex tasks. The other possible direction is to find a solution that can automatically decide the optimal set of sensors selected for control.

7 ACKNOWLEDGEMENT

This work was supported by the National Science Foundation of China (61772473, 62073345 and 62011530148). F. Wang was supported by the Equipment Pre-research Key Laboratory Funds No. 61425010102.

REFERENCES

- [1] Joshua Achiam. 2018. Spinning Up in Deep Reinforcement Learning. (2018).
- [2] Martin Alnæs, Jan Blechta, Johan Hake, August Johansson, Benjamin Kehlet, Anders Logg, Chris Richardson, Johannes Ring, Marie E Rognes, and Garth N Wells. 2015. The FEniCS project version 1.5. *Archive of Numerical Software* 3, 100 (2015).
- [3] Yoshua Bengio, Aaron Courville, and Pascal Vincent. 2013. Representation learning: A review and new perspectives. *IEEE transactions on pattern analysis and machine intelligence* 35, 8 (2013), 1798–1828.
- [4] Leo Breiman. 2001. Random forests. *Machine learning* 45, 1 (2001), 5–32.
- [5] Ido Bright, Guang Lin, and J Nathan Kutz. 2013. Compressive sensing based machine learning strategy for characterizing the flow around a cylinder with limited pressure measurements. *Physics of Fluids* 25, 12 (2013), 127102.
- [6] Greg Brockman, Vicki Cheung, Ludwig Pettersson, Jonas Schneider, John Schulman, Jie Tang, and Wojciech Zaremba. 2016. Openai gym. *arXiv preprint arXiv:1606.01540* (2016).
- [7] Jianbo Chen, Le Song, Martin Wainwright, and Michael Jordan. 2018. Learning to explain: An information-theoretic perspective on model interpretation. In *International Conference on Machine Learning*. PMLR, 883–892.
- [8] Jianbo Chen, Mitchell Stern, Martin J Wainwright, and Michael I Jordan. 2017. Kernel feature selection via conditional covariance minimization. *Advances in Neural Information Processing Systems* 30 (2017).
- [9] Tianqi Chen and Carlos Guestrin. 2016. Xgboost: A scalable tree boosting system. In *Proceedings of the 22nd acm sigkdd international conference on knowledge discovery and data mining*. 785–794.
- [10] Po-Wei Chou. 2017. *The Beta Policy for Continuous Control Reinforcement Learning*. Master's thesis. Carnegie Mellon University, Pittsburgh PA.
- [11] Kelly Cohen, Stefan Siegel, and Thomas McLaughlin. 2006. A heuristic approach to effective sensor placement for modeling of a cylinder wake. *Computers & fluids* 35, 1 (2006), 103–120.
- [12] Mengnan Du, Ninghao Liu, Qingquan Song, and Xia Hu. 2018. Towards explanation of dnn-based prediction with guided feature inversion. In *Proceedings of the 24th ACM SIGKDD International Conference on Knowledge Discovery & Data Mining*. 1358–1367.
- [13] Quanquan Gu, Zhenhui Li, and Jiawei Han. 2011. Generalized Fisher score for feature selection. In *Proceedings of the Twenty-Seventh Conference on Uncertainty in Artificial Intelligence*. 266–273.
- [14] Ning Gui, Danni Ge, and Ziyin Hu. 2019. AFS: An attention-based mechanism for supervised feature selection. In *Proceedings of the AAAI Conference on Artificial Intelligence*, Vol. 33. 3705–3713.
- [15] Tin Kam Ho. 1995. Random decision forests. In *Proceedings of 3rd international conference on document analysis and recognition*, Vol. 1. IEEE, 278–282.
- [16] RL Hu, J Granderson, DM Auslander, and A Agogino. 2019. Design of machine learning models with domain experts for automated sensor selection for energy fault detection. *Applied energy* 235 (2019), 117–128.
- [17] Guolin Ke, Qi Meng, Thomas Finley, Taifeng Wang, Wei Chen, Weidong Ma, Qiwei Ye, and Tie-Yan Liu. 2017. Lightgbm: A highly efficient gradient boosting decision tree. *Advances in neural information processing systems* 30 (2017), 3146–3154.
- [18] Udayan Khurana, Horst Samulowitz, and Deepak Turaga. 2018. Feature engineering for predictive modeling using reinforcement learning. In *Proceedings of the AAAI Conference on Artificial Intelligence*, Vol. 32.
- [19] Alexander Kuhnle, Michael Schaarschmidt, and Kai Fricke. 2017. Tensorforce: a TensorFlow library for applied reinforcement learning. Web page. <https://github.com/tensorforce/tensorforce>
- [20] Jundong Li, Kewei Cheng, Suhang Wang, Fred Morstatter, Robert P Trevino, Jiliang Tang, and Huan Liu. 2017. Feature selection: A data perspective. *ACM Computing Surveys (CSUR)* 50, 6 (2017), 1–45.
- [21] Timothy P Lillicrap, Jonathan J Hunt, Alexander Pritzel, Nicolas Heess, Tom Erez, Yuval Tassa, David Silver, and Daan Wierstra. 2016. Continuous control with deep reinforcement learning. In *ICLR (Poster)*.
- [22] Volodymyr Mnih, Koray Kavukcuoglu, David Silver, Andrei A Rusu, Joel Veness, Marc G Bellemare, Alex Graves, Martin Riedmiller, Andreas K Fidjeland, Georg Ostrovski, et al. 2015. Human-level control through deep reinforcement learning. *nature* 518, 7540 (2015), 529–533.
- [23] Stephan F Oehler and Simon J Illingworth. 2018. Sensor and actuator placement trade-offs for a linear model of spatially developing flows. *Journal of Fluid Mechanics* 854 (2018), 34–55.
- [24] Romain Paris, Samir Beneddine, and Julien Dandois. 2021. Robust flow control and optimal sensor placement using deep reinforcement learning. *Journal of Fluid Mechanics* 913 (2021).
- [25] Fabian Pedregosa, Gaël Varoquaux, Alexandre Gramfort, Vincent Michel, Bertrand Thirion, Olivier Grisel, Mathieu Blondel, Peter Prettenhofer, Ron Weiss, Vincent Dubourg, et al. 2011. Scikit-learn: Machine learning in Python. *the Journal of machine Learning research* 12 (2011), 2825–2830.
- [26] Jean Rabault, Miroslav Kuchta, Atle Jensen, Ulysse Réglade, and Nicolas Cerardi. 2019. Artificial neural networks trained through deep reinforcement learning discover control strategies for active flow control. *Journal of Fluid Mechanics* 865 (2019), 281–302.
- [27] Jean Rabault and Alexander Kuhnle. 2019. Accelerating deep reinforcement learning strategies of flow control through a multi-environment approach. *Physics of Fluids* 31, 9 (2019), 094105.
- [28] Marko Robnik-Šikonja and Igor Kononenko. 2003. Theoretical and empirical analysis of ReliefF and RReliefF. *Machine learning* 53, 1 (2003), 23–69.
- [29] Wojciech Samek, Thomas Wiegand, and Klaus-Robert Müller. 2017. Explainable artificial intelligence: Understanding, visualizing and interpreting deep learning models. *arXiv preprint arXiv:1708.08296* (2017).
- [30] Michael Schäfer, Stefan Turek, Franz Durst, Egon Krause, and Rolf Rannacher. 1996. Benchmark computations of laminar flow around a cylinder. In *Flow simulation with high-performance computers II*. Springer, 547–566.
- [31] John Schulman, Filip Wolski, Prafulla Dhariwal, Alec Radford, and Oleg Klimov. 2017. Proximal policy optimization algorithms. *arXiv preprint arXiv:1707.06347* (2017).
- [32] Blaž Škrlj, Sašo Džeroski, Nada Lavrač, and Matej Petkovič. 2020. Feature importance estimation with self-attention networks. *arXiv preprint arXiv:2002.04464* (2020).
- [33] Richard S Sutton and Andrew G Barto. 2018. *Reinforcement learning: An introduction*. MIT press.
- [34] Hongwei Tang, Jean Rabault, Alexander Kuhnle, Yan Wang, and Tongguang Wang. 2020. Robust active flow control over a range of Reynolds numbers using an artificial neural network trained through deep reinforcement learning. *Physics of Fluids* 32, 5 (2020), 053605.
- [35] Jiliang Tang, Salem Alelyani, and Huan Liu. 2014. Feature selection for classification: A review. *Data classification: Algorithms and applications* (2014), 37.
- [36] Maksymilian Wojtas and Ke Chen. 2020. Feature importance ranking for deep learning. *Advances in Neural Information Processing Systems* 33 (2020), 5105–5114.
- [37] Kui Yu, Lin Liu, and Jiuyong Li. 2021. A Unified View of Causal and Non-causal Feature Selection. *ACM Transactions on Knowledge Discovery from Data (TKDD)* 15, 4 (2021), 1–46.

APPENDIX A: THE EXPERIMENTAL RESULTS OF OPENAI GYM

Since our method has good scalability and can minimize the changes to the existing DRL algorithm, we apply the architecture to two mainstream algorithms, DQN and DDPG. We apply D-AFS/DQN and D-AFS/DDPG to four classical control environments provided by OpenAI Gym, the Pendulum, MountainCar, CartPole, and Acrobot. The four target systems are shown in Fig. A1, and the weights generated by D-AFS are shown in Table A1. The boldface in the table indicates the features selected by D-AFS. "P_Ran" and "Ran" represent partial noise and complete noise, respectively. The results show that our method can effectively select the most relevant sensors and reduce human expertise reliance.

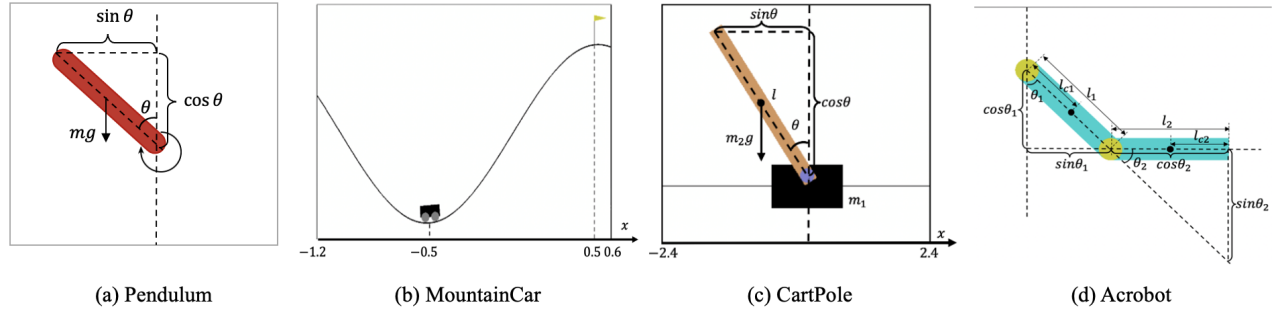


Figure A1: The physical meaning of the major features in the four systems

Table A1: Results of D-AFS in four classical control systems provided OpenAI Gym

Algorithm	Systems	All inputs and weights										
D-AFS/DQN	Pendulum	θ	ω	$\sin \theta$	$\cos \theta$	P_Ran	Ran					
		0.516	0.968	0.960	0.879	1.27e-4	2.32e-5					
	MountainCar	x	v	P_Ran	Ran							
		0.862	0.828	7.99e-5	1.75e-4							
	CartPole	x	v	θ	ω	$\sin \theta$	$\cos \theta$	P_Ran	Ran			
		0.618	0.601	0.047	0.952	0.997	0.955	2.28e-4	9.57e-4			
	Acrobot	θ_1	θ_2	ω_1	ω_2	$\sin \theta_1$	$\cos \theta_1$	$\sin \theta_2$	$\cos \theta_2$	P_Ran	Ran	
		0.907	0.407	0.921	0.470	0.356	0.965	0.809	0.848	1.04e-3	1.95e-3	
			0.408	0.427	0.934	0.537	0.674	0.938	0.658	0.924	1.75e-3	2.79e-3
	D-AFS/DDPG	Pendulum	θ	ω	$\sin \theta$	$\cos \theta$	P_Ran	Ran				
0.243			0.561	0.956	0.739	1.20e-3	2.96e-3					
MountainCar		x	v	P_Ran	Ran							
		0.178	0.894	3.48e-4	3.27e-4							
CartPole		x	v	θ	ω	$\sin \theta$	$\cos \theta$	P_Ran	Ran			
		0.822	0.386	0.955	0.356	0.868	0.607	0.009	0.002			
Acrobot		θ_1	θ_2	ω_1	ω_2	$\sin \theta_1$	$\cos \theta_1$	$\sin \theta_2$	$\cos \theta_2$	P_Ran	Ran	
		0.651	0.459	0.273	0.302	0.609	0.754	0.785	0.821	2.67e-3	2.16e-3	